Regressive tomography and direct regressive reconstruction: a research note

Henri WEISEN[1], Jari VARJE[2], Paula SIRÉN[3], Zamir GHANI[3] and JET CONTRIBUTORS[*]

[1]Ecole Polytechnique Fédérale de Lausanne (EPFL), Swiss Plasma Center (SPC), Lausanne, Switzerland

[2]Aalto University, Espoo, Finland

[3]CCFE, Culham Science Centre, Abingdon, Oxon, OX14 3DB, United Kingdom

*See the author list of :"Overview of JET results for optimising ITER operation", by J. Mailloux 2022 Nucl. Fusion, https://doi.org/10.1088/1741-4326/ac47b4

Corresponding author:

Henri Weisen, chemin de Gravernay 14, CH-1030 Bussigny, Switzerland

Tel: +44 777 263 3953

Email: henri.weisen@alumni.epfl.ch

Regressive tomography and direct regressive reconstruction: a research note

H. WEISEN[1], J. VARJE[2], P. SIRÉN[3], Z. GHANI[3] and JET CONTRIBUTORS[*]

[1]Ecole Polytechnique Fédérale de Lausanne (EPFL), Swiss Plasma Center (SPC), Lausanne, Switzerland

[2]Aalto University, Espoo, Finland

[3]CCFE, Culham Science Centre, Abingdon, Oxon, OX14 3DB, United Kingdom

*See the author list of :"Overview of JET results for optimising ITER operation", by J. Mailloux 2022 Nucl. Fusion, https://doi.org/10.1088/1741-4326/ac47b4

Abstract: Two related methods for inverting line integrated measurements are presented in this research note in the context of the recent Deuterium-Tritium experiments in the JET tokamak. Unlike traditional methods of tomography, these methods rely on making use of a family of model distributions defining a functional space within which a solution of the inversion problem is expected to exist. This is a stronger assumption than that underlying traditional methods of tomography and requires that suitable models for the expected distribution are available. In return, the methods offer computationally efficient and robust reconstructions. Regressive tomography, as applied to the data from the JET neutron cameras, involves calculating a set of 100 or more 2D neutron emission distributions in a representative variety of conditions using the ASCOT and AFSI Monte Carlo fast ion orbit and fusion reaction codes. The distributions are line-integrated to represent synthetic measurements from the 19 channels of this two camera system. An inversion matrix is then obtained by regressing the 2D distributions corresponding to each of the voxels against these line integrals. The second method, direct regressive reconstruction, bypasses the calculation of line integrals altogether by regressing experimental camera data against calculated neutron emission distributions. This method does not require the cameras to be calibrated, not even relatively between channels. The inversion matrices obtained by any of the two methods can then

be used to provide neutron emission profiles for which ASCOT/AFSI calculations are not available.

I. Introduction

A major motivation for inferring the neutron emission distribution is the fact that it coincides with the alpha particle source distribution from deuterium-tritium (DT) fusion reactions. Alpha particles will play many roles in future burning plasma devices, such as plasma self-heating, driving potentially deleterious energetic particle instabilities[1], as well as reducing heat transport by stabilising ion temperature gradient turbulence[2]. JET is equipped with a horizontal and a vertical neutron camera[3,4] and three fission chambers for monitoring the total neutron rate[5,6]. The cameras consist of two fan-shaped arrays of detectors, as shown in fig. 1, with ten horizontal and nine vertical lines of sight for a total of 19 channels, which are enough to perform tomographic inversion and therefore to derive information about the spatial distribution of the neutron emission[7-12].

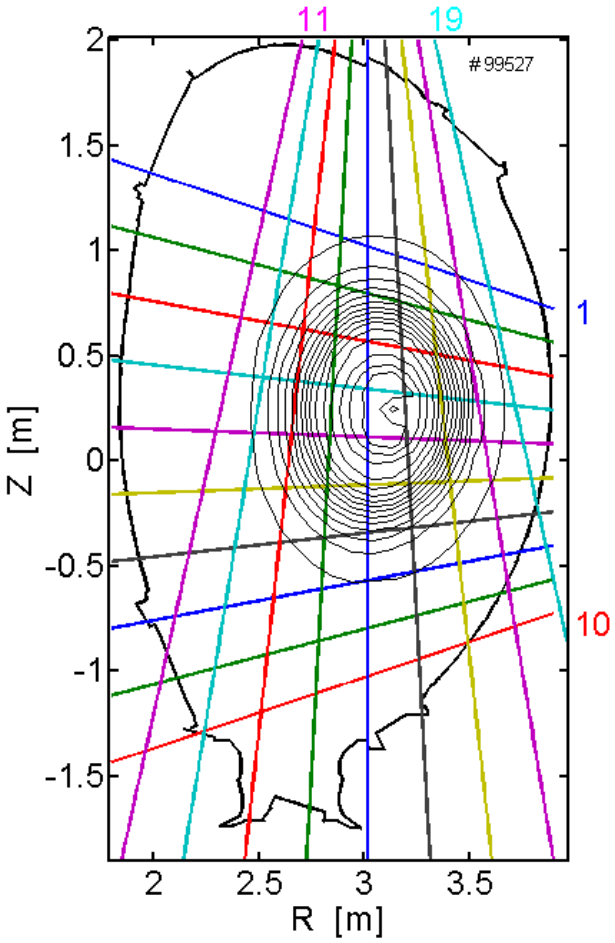

Fig.1. Geometry of viewing lines of the JET neutron cameras. The contour lines correspond to the DT neutron emission distribution from an ASCOT/AFSI simulation of DT pulse number 99527.

Each line of sight is equipped with two detectors: a NE213 detector which can measure both the 2.45 and the 14 MeV neutrons and a Bicron detector for the 14 MeV neutrons. The energy selection is performed using threshold discrimination. The neutron emission by JET plasmas has been extensively modelled using the ASCOT code[13,14] and the AFSI (ASCOT Neutron Source Integrator) code[15-17], which uses ASCOT output particle velocity distributions to calculate the nuclear reactions between ion species, i.e. the local DT neutron rates for the case of this study. Tokamak plasmas are close to axi-symmetrical around the toroidal (vertical) axis. The ASCOT and AFSI codes, as applied to tokamaks, assume axi-symmetric distributions of plasma parameters such as temperatures and densities and provide neutron emissivities in neutrons/m^3/s as function of the

horizontal and vertical coordinates R and Z. Even though only 1000 tracer particles were used for the ASCOT calculations, it took about 10 minutes on the JET computers to produce each of the neutron emission distributions used in this study. For systematic evaluations of the neutron emissivity this is unpractically slow, motivating the usage of faster methods.

II. Regressive tomography (RT)

The dataset used here is a set of 1563 ASCOT/AFSI calculations in Deuterium-Tritium (DT) plasmas. These were not specifically created for the purpose of creating the set used to develop the methods presented here. Part of the set was produced with the aim of extrapolating from deuterium plasmas to DT plasmas[18], another part was produced in investigations of the D minority fraction in dominantly Tritium or Tritium-Hydrogen plasmas and part was produced for modelling DT plasmas produced during the DTE2 Deuterium-Tritium campaign (August-December 2022). The results of these DT ASCOT calculations are part of ~7000 ASCOT calculations so far produced and part of the previously described JETPEAK database and analysis environment[17,19]. These DT neutron emission profiles E(R,Z) are provided by AFSI on a 26x51 R-Z grid (major radius - elevation, 1.66m≤R≤4.04 m, -1.89≤Z≤2.14m), defining 25x50 voxels (toroidal volume elements of volume $2\pi R\Delta R\Delta Z$, where ΔR and ΔZ are the horizontal and vertical grid spacings). The lines of sight of the neutron cameras shown in fig.1. The line integrals of these distributions were evaluated along the camera lines of sight, yielding the neutron fluxes (neutrons/m^2/s) expected for the different channels, $I_k = \int E_k(l_k)dl$. The line integrals extend over the viewing lines corresponding to the channels indexed by k. $E_k(l_k)$ was obtained by a 2D interpolation of the discrete local emissivities E_{ij} onto the lines of sight. Here, i indexes the radial coordinate and j the vertical one. The next step consisted in producing linear regressions[20] for the local emissivity E_{ij}. The standard Matlab[21] regression function "regress.m" was then used without an additive constant to produce a matrix of regression coefficients b_{ijk} such that

$$F_{ij} = \sum_{k=1}^{n} b_{ijk} I_k \qquad \text{eq.1}$$

where F_{ij} are the reconstructed emissivities, k indexes the n=19 detector channels, b_{ijk} being the regression coefficient obtained for channel k and the spatial position indexed by ij. In the example

shown in fig.2, 147 randomly selected samples were selected for creating the matrix b_{ijk} and the remaining 1416 for testing the quality of the regression on a set different from the input set. (In practice, the dimensions corresponding to i and j are reshaped into a single one, yielding a 2D matrix). It is worthwhile stressing that emissivities at all positions are independently reconstructed. No smoothing or regularisation is applied.

The method described here is similar to the practice of using different training and prediction sets for neural network based reconstructions[22-24]. The difference is that we are using a standard linear algebra tool for what might be termed 'linear training', which is appropriate here, as the tomography problem is linear. Neural networks are widely used together with linear methods for a great variety of inverse problems[25-27]. When inverse problems are amenable to linear reconstruction, linear methods, such as regressions, offer convenient benchmarks for the far more complex machine learning methods. In most cases the training is performed on available data in order to provide predictions for cases for which data are not available. The method described here for neutron tomography in a fusion plasma is a case where instead of available experimental data, we use modelled data. Indeed, there exists no possibility for creating an experimental dataset of locally measured neutron birth rates in the hot interior of a fusion plasma.

The regressed emissivities F_{ij} are shown in fig.2, a-d, for 4 positions along a vertical line near the middle of the vessel (R=3.07) versus the original local emissivities E_{ij}. The standard deviations of F_{ij} from E_{ij} are typically a few percent of the mean values of E_{ij}, which can be considered as satisfactory. Fig.2e shows the 1416 reconstructions plotted on top of each other and fig.2f depicts the 147 'linear training' distributions having served to obtain the matrix b_{ijk}. A similar quality of reconstruction is obtained for all voxels.

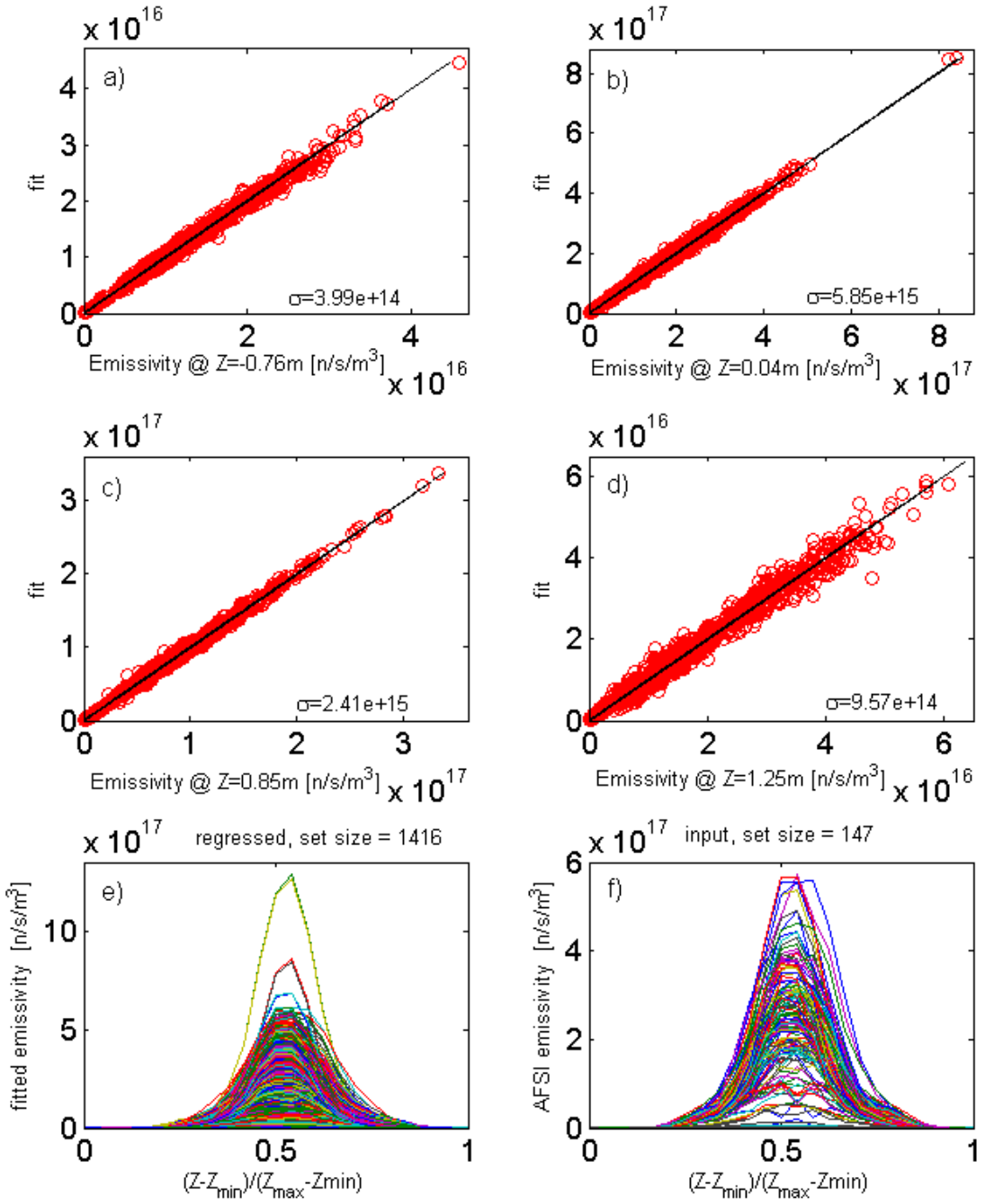

Fig.2. a-d) Regressed vs original emissivities from ASCOT/AFSI for 4 voxels along a vertical line through the middle of the JET vessel. ***σ*** *is the standard deviation of* F_{ij} *-* E_{ij}*. e) vertical cut at R= 3.04m in normalised vertical coordinates for all reconstructed emissivities f) vertical cut for all emissivity distributions having been used to create the inversion matrix.*

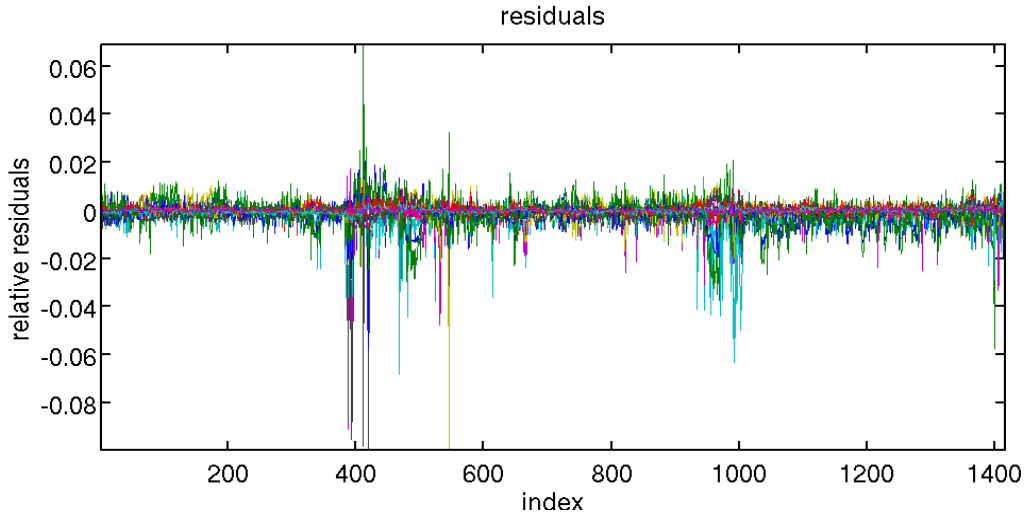

Fig.3. Relative residuals for all of the reconstruction and all of the 19 channels, superimposed. The horizontal axis refers to the sample number.

Fig.3 shows the relative residuals of the 1416 reconstructions for all channels, plotted on top of each other. It is immediately apparent that the residuals are typically of order 1% with exceptions in a handful of cases where residuals exceed 5%. In the first attempts these cases were more numerous and were even larger. We found that they correspond to cases with emissivities as low as 1-3% which were obtained when simulating neutron emission in T plasmas with 1% of residual deuterium. These appear to have had profile shapes differing somewhat from the higher emission cases obtained assuming 50/50 D-T mixtures. At these low levels they had negligible weight in the regression and hence suffered 'regressive neglect'. This effect was mitigated by including copies of these cases simply scaled up linearly to the average emissivity.

The count rates from the bicron detectors, which are best suited for DT neutrons, were used for this study. We limited these to 420 cases obtained during the DT campaign with total neutron rates above ~$2\text{x}10^{16}$ n/s. Following the production of the inversion matrix b_{ijk} the first attempts to reconstruct experimental neutron emission profiles based on experimental count rates J_k from the JET neutron cameras faced the difficulty that the system was uncalibrated. An independent

calibration would require modelling the entire JET vessel together with the neutron camera hardware and detectors using a neutron transport code such as MCNP [Ref. 28] and a detector description and simulation tool such as GEANT [Ref. 29]. Such an undertaking is beyond the scope of this research note. The absence of a channel-to-channel relative calibration was immediately apparent from plotting the ratio I_k/J_k of the expected line integral I_k to the measured one J_k, as well as from the rugged appearance of the reconstructions. As a result I_k/J_k averaged over a large number of samples, was used to create an ad hoc calibration function shown in fig.4.

Using this calibration acceptable reconstructions were obtained, as seen in fig.5. Some artefacts likely due to an imperfect ad-hoc calibration appear to persist in the vertical slice shown in fig.5a. As the reconstructions were produced directly from the measured count rates, the vertical axes in fig.5 do not have the meaning of neutron emissivities in n/s/m^3. Local emissivities however can be obtained by scaling the reconstructions such that the volume integral for each sample matches the total neutron rate provided by the fission chambers, amounting to a calibration of the camera system by the fission chambers.

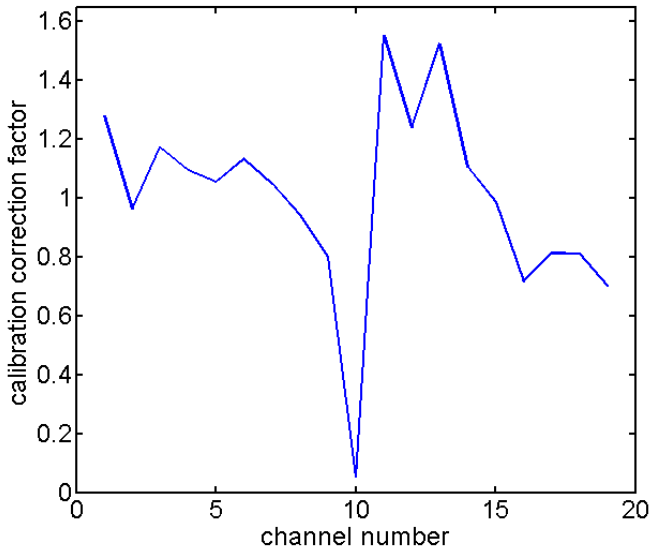

Fig.4. Correction factor applied to the experimental neutron camera count rates as an ad-hoc calibration.

At total DT neutron rates rates above 10^{18} n/s pile-up corrections for the measured count rates were clearly required. Pulse pile-up corrections factors are provided as part of the publication of the neutron camera data in the JET processed pulse files. These too have an important effect, as errors in the treatment of pile-up would also lead to reconstruction errors, although to the extent of the above

lack of calibration. We also devised and applied an empirical pile-up correction obtained from scaling of the raw count rates with the total neutron rate. The empirical pile-up leads to reconstructions with marginally lower residuals. The relative residuals for the camera channels with the highest count rates (3-6 and 13-17) have residuals in the range 1-3%, except for a handful of outliers.

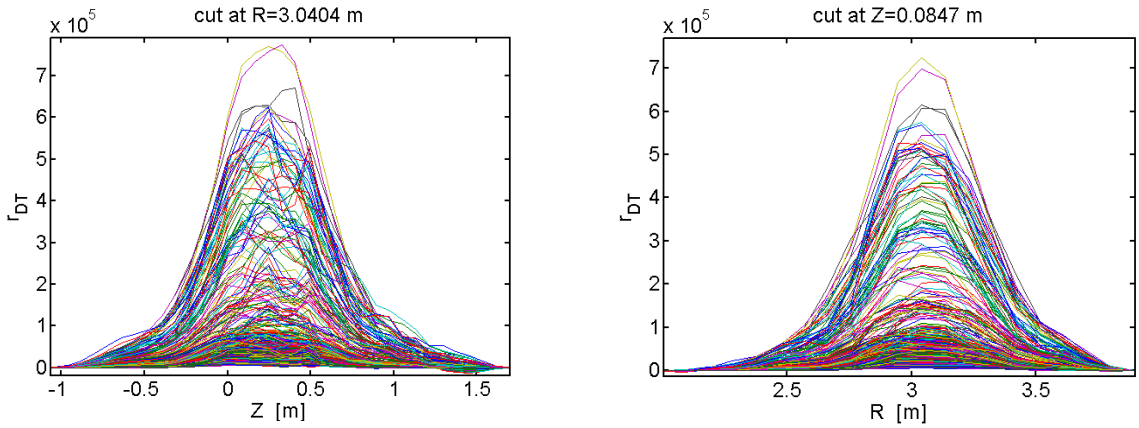

Fig.5. Regressive tomographic reconstructions obtained with an empirical calibration of the channel-to-channel count rates. left: vertical slice, right: horizontal slice

Peripheral channels have residuals of order 5% and higher. For some channels residuals are biassed towards positive or negative values, suggesting the channel-to-channel calibration still needs improving. This observation suggests that channel-to-channel calibration may be improved iteratively with the aim of removing bias in the residuals.

III. Direct regressive reconstruction (DRR)

The necessity of an ad hoc calibration using modelled data may seem disappointing, but also suggests a one-step reconstruction method that does not require a relative calibration in the first place. This method is already in use at JET for 1D profile data, such as ion temperature and rotation profiles when only sparse measurements are available and is here extended to 2D reconstructions. To this effect a sufficient number of modelled cases need to be available together with experimental measurements. The modelled 2D distributions E_{ij} are regressed directly against the measured count rates J_k , producing a matrix of coefficients c_{ijk} such that

$$F_{ij} = \sum_{k=1}^{n} c_{ijk} J_k \qquad \text{eq.2}$$

where F_{ij} is the reconstructed emission at voxel i,j.

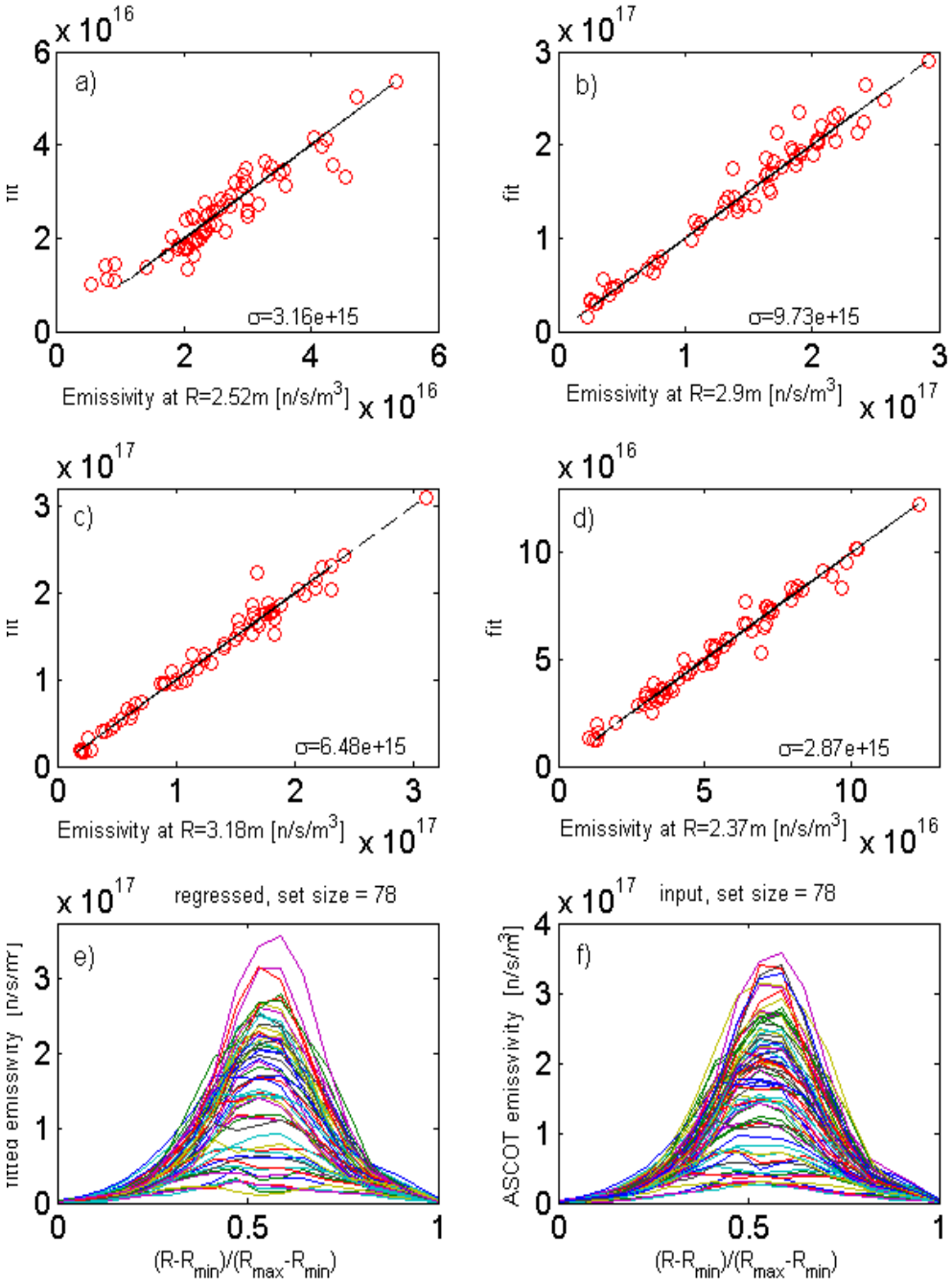

Fig.6. a-d) Direct regressive reconstructions of emissivity profiles versus the original emissivities calculated by ASCOT (horizontal slice at Z=0.4 m). e) full reconstructed distributions f) original distributions. In e) and f) the horizontal axis is in normalised vertical coordinates.

As this method does not involve the calculation of any line integrals, nor the availability of a calibration, we cannot call this method ‘tomography’. Fig.6 shows for 76 cases from the DT campaign how well reconstructions using this method, direct regressive reconstruction (DRR), match the modelled originals. The model profiles were normalised to the total neutron rate. Differences are typically 5% of the mean values and residuals, with a few exceptions, are below 10%. While residuals are higher than with regressive tomography, this method has the advantage that relative calibration errors have no influence and hence cannot introduce artefacts due to calibration errors. Another advantage may be that this method is also insensitive to the influence of back-scattered neutrons, as their contribution to the detected count rates is also linearly related to the plasma emissivity. We speculate that the DRR method may be more sensitive than RT to a mismatch between the experimental training set and the corresponding model set, as it lacks the explicit relationship imposed by the line integrals, between the local emissivities and the detector signals.

IV. Discussion

While both the relative calibration and the processing of pulse pile-up of the JET neutron cameras deserve further attention, the two methods presented clearly possess potential for applications to 2D reconstructions. In comparison with ASCOT calculations they are considerably faster, as they rely on matrix multiplications which take milliseconds to perform rather than minutes. These are “forward” methods, rather than “inverse” methods, as are the traditional tomographic methods[5-10]. Unlike inverse methods, the two linear regressive methods presented rely on the adequacy and quality of the forward model used to generate the regressions. The advantage is that adopting a forward method greatly reduces the space of possible solutions to those which are allowed by the training set used, thereby reducing the likelihood for artefacts in the reconstructions. In the case of neutron tomography, as can easily be seen in figures 2.f) and 6.f), the solutions are fairly featureless and characterised by distributions that are peaked in the plasma core. This is appropriate, as fusion reactivities drop sharply with plasma temperature, leading to neutron emissivities decreasing

sharply with distance from the plasma centre. There is generally no need to allow for flat or hollow profiles or for isolated emissive regions, as in the case of electromagnetic radiation measured using bolometer cameras[22-24]. It remains to be seen how tolerant the methods are to using different sets of distributions, e.g. ad hoc sets not produced by ASCOT/AFSI. A set not representative of the physical reality in the plasma is likely to lead to incorrect and biassed reconstructions. These would probably be recognisable by large residuals, triggering a search for a more suitable training set, or the adoption of a different method. Further work, which is beyond the scope of this research note, should aim at exploring the tolerance to less than adequate forward models, as well as to comparing them with other reconstruction methods.

Acknowledgement

This work has been carried out within the framework of the EUROfusion Consortium and has received funding from the Euratom research and training programme 2014-2018 and 2019-2020 under grant agreement No 633053. The views and opinions expressed herein do not necessarily reflect those of the European Commission.

References

1. N.N. GOROLENKOV et al., Nucl. Fusion **54**, (2014) 125001
2. J. GARCIA and JET CONTRIBUTORS, Plasma Phys. Control. Fusion, **64** (2022) 104002
3. J.M. ADAMS et al., Nucl. Instrum. Meth., **A 329**, 277, 1993
4. A. MURARI et al,, Rev. of Sci. Instrum. **81**, 10E136, 2010
5. M.T . SWINHOE and O.N. JARVIS, Rev. Sci . Instr., **56**, 1093, 1985
6. P. BATISTONI et al., Nucl. Fusion, **58**, 106016, 2018
7. F. B. MARCUS et al., Plasma Phys. Control. Fusion, **33**, 277, 1991
8. G. BONHEURE et al., 2006 Nucl. Fusion, **46**, 725, 2006
9. T. CRACIUNESCU et al., Nuclear Instruments and Methods in Physics Research, **A 595**,

623–630, 2008

10. T. CRACIUNESCU et al., Nuclear Instruments and Methods in Physics Research, **A 605**, 374–383, 2009
11. E. RONCHI et al., Nucl. Fusion, **50,** 035008, 2010
12. J. MLYNAR et al., Journal of Fusion Energy, **38**, 458–466, 2019
13. E. HIRVIJOKI et al., Comput. Phys. Commun., **185** 1310-1321, 2014
14. O. ASUNTA et al., Comput. Phys. Commun., **188** 33-46, 2015
15. P. SIRÉN et al., JINST, **12**, C09010, 2017
16. P. SIRÉN et al., Fusion Eng. Des., **146**, 2019, 1587-1590,
17. P. SIRÉN et al., JINST **14** (2019) C11013
18. H. WEISEN et al., Nucl. Fusion, **61** (2021) 124002
19. H. WEISEN et al., Nucl. Fusion, **60** (2020) 036004
20. O.J.W.F. KARDAUN, Classical Methods of Statistics (Berlin: Springer), ISBN-10 3-540-2115-2, 2005
21. The MathWorks, Inc., https://uk.mathworks.com/products/matlab.html
22. F.A. MATOS et al., Fusion Eng. Des., **114** (2017) 18–25
23. D.D. CARVALHO et al., JINST **14**, (2019) C09011
24. D.R. FERREIRA et al., Fusion Eng. Des., **164** (2021), 112179
25. J. CHEN et al., Environment International **130** (2019) 104934
26. M. T. McCANN, K. H. JIN and M. UNSER, "Convolutional Neural Networks for Inverse Problems in Imaging: A Review," in *IEEE Signal Processing Magazine*, **34**, (2017) 85-95, https://doi.org/10.48550/arXiv.1710.04011
27. B. YEDDER et al., "Deep Learning Based Image Reconstruction for Diffuse Optical Tomography". In: Knoll, F., Maier, A., Rueckert, D. (eds) Machine Learning for Medical Image Reconstruction. MLMIR (2018) 112–119. *Lecture Notes in Computer Science* (2018), vol 11074, . Springer, Cham., https://doi.org/10.1007/978-3-030-00129-2_13
28. B. KIEDROWSKI et al., M. C. N. P. Documentation. "MCNP5-1.6, Feature Enhancements and Manual Clarifications." LA-UR-l0-06217 (2010).

29. CERN Program Library Long Writeup W5013, “GEANT Detector Description and Simulation Tool”, CERN Program Library Office CERN-IT Division, CH-1211 Geneva 23, Switzerland. https://cds.cern.ch/record/1073159/files/cer-002728534.pdf

Figure captions

Fig.1. Geometry of viewing lines of the JET neutron cameras. The contour lines correspond to the DT neutron emission distribution from an ASCOT/AFSI simulation of DT pulse number 99527.

Fig.2. a-d) Regressed vs original emissivities from ASCOT/AFSI for 4 voxels along a vertical line through the middle of the JET vessel. $\boldsymbol{\sigma}$ *is the standard deviation of* F_{ij} - E_{ij}*. e) vertical cut at R= 3.04m in normalised vertical coordinates for all reconstructed emissivities f) vertical cut for all emissivity distributions having been used to create the inversion matrix.*

Fig.3. Relative residuals for all of the reconstruction and all of the 19 channels, superimposed. The horizontal axis refers to the sample number.

Fig.4. Correction factor applied to the experimental neutron camera count rates as an ad-hoc calibration.

Fig.5. Regressive tomographic reconstructions obtained with an empirical calibration of the channel-to-channel count rates. left: vertical slice, right: horizontal slice

Fig.6. a-d) Direct regressive reconstructions of emissivity profiles versus the original emissivities calculated by ASCOT (horizontal slice at Z=0.4 m). e) full reconstructed distributions f) original distributions. In e) and f) the horizontal axis is in normalised vertical coordinates.